



THE UNIVERSITY *of* EDINBURGH

Edinburgh Research Explorer

FIM2c : A Multi-Colour, Multi-Purpose Imaging System to Manipulate and Analyse Animal Behaviour

Citation for published version:

Risse, B, Otto, N, Berh, D, Jiang, X, Kiel, M & Klambt, C 2017, 'FIM2c : A Multi-Colour, Multi-Purpose Imaging System to Manipulate and Analyse Animal Behaviour', *IEEE Transactions on Biomedical Engineering*, vol. 64, no. 3, pp. 1-11. <https://doi.org/10.1109/TBME.2016.2570598>

Digital Object Identifier (DOI):

[10.1109/TBME.2016.2570598](https://doi.org/10.1109/TBME.2016.2570598)

Link:

[Link to publication record in Edinburgh Research Explorer](#)

Document Version:

Peer reviewed version

Published In:

IEEE Transactions on Biomedical Engineering

General rights

Copyright for the publications made accessible via the Edinburgh Research Explorer is retained by the author(s) and / or other copyright owners and it is a condition of accessing these publications that users recognise and abide by the legal requirements associated with these rights.

Take down policy

The University of Edinburgh has made every reasonable effort to ensure that Edinburgh Research Explorer content complies with UK legislation. If you believe that the public display of this file breaches copyright please contact openaccess@ed.ac.uk providing details, and we will remove access to the work immediately and investigate your claim.



FIM^{2c}: A Multi-Colour, Multi-Purpose Imaging System to Manipulate and Analyse Animal Behaviour

Benjamin Risse*, Member, IEEE, Nils Otto*, Dimitri Berh, Xiaoyi Jiang[†], Senior Member, IEEE, Matthias Kiel, and Christian Klämbt

Abstract—In vivo whole-body imaging of small animals plays an important role for biomedical studies. In particular, animals like the fruit fly *Drosophila melanogaster* or the nematode *Caenorhabditis elegans* are popular model organisms for pre-clinical research since they offer sophisticated genetic tool-kits. Recording these translucent animals with high contrast in a large arena is however not trivial. Furthermore fluorescent proteins are widely used to mark cells in vivo and report their functions. This paper introduces a novel optical imaging technique called FIM^{2c} enabling simultaneous detection of the animals posture and movement as well as fluorescent markers like GFP. FIM^{2c} utilizes frustrated total internal reflection of two distinct wavelengths and captures both, reflected and emitted light. The resultant two-colour high-contrast images are superb compared to other imaging systems for larvae or worms. This multi-purpose method enables a large variety of different experimental approaches. For example FIM^{2c} can be used to image GFP positive cells / tissues / animals and supports the integration of fluorescent tracers into multi-target tracking paradigms. Moreover, optogenetic tools can be applied in large scale behavioural analysis to manipulate and study neuronal functions. To demonstrate the benefit of our system, we use FIM^{2c} to resolve colliding larvae in a high-throughput approach, which was impossible given the existing tools. Finally, we present a comprehensive database including images and locomotion features of more than 1,300 resolved collisions available for the community. In conclusion FIM^{2c} is a versatile tool for advanced imaging and locomotion analysis for a variety of different model organisms.

Index Terms—Imaging Technique, Tracking, Behavioural Experiments, *Drosophila* Larvae, *C. elegans*, GFP, FIM, Optogenetics, Neuro Science, Collisions

I. INTRODUCTION

BEHAVIORAL studies of animals like worms, larvae or beetles have become an integral subject of biological research. Examples are *Drosophila melanogaster* [1]–[3] or the

B. Risse, D. Berh and X. Jaing are with the Department of Mathematics and Computer Science, University of Münster, Einsteinstr. 62, 48149 Münster, Germany, e-mail: b.risse@uni-muenster.de, d.berh@uni-muenster.de, xjiang@uni-muenster.de

N. Otto and C. Klämbt are with the Department of Behaviour and Neuronal Biology, University of Münster, Badestr. 9, 48149 Münster, Germany, e-mail: nils.otto@uni-muenster.de, klaembt@uni-muenster.de

M. Kiel is with the Research Group Microbial Genome Plasticity, University Hospital Münster, Robert-Koch-Str. 41, 48149 Münster, Germany, e-mail: matt.schreiner@uni-muenster.de

Authors marked by * contribute equally and the corresponding author is marked by †.

Copyright (c) 2016 IEEE. Personal use of this material is permitted. However, permission to use this material for any other purposes must be obtained from the IEEE by sending an email to pubs-permissions@ieee.org.

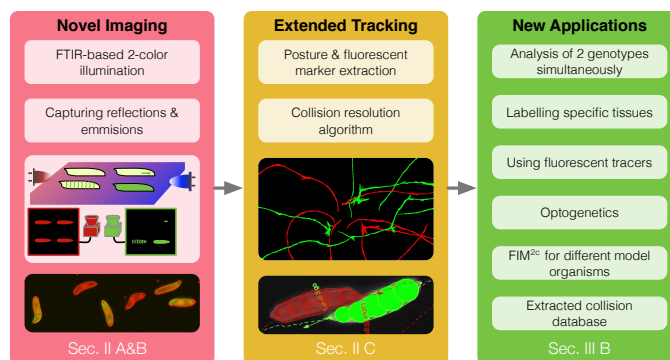


Fig. 1. System layout and overview of our contributions. First, we use a novel imaging technique called FIM^{2c} to extract the posture and fluorescent markers of freely crawling animals. In a second step we implemented several algorithms to quantify the locomotion and the fluorescence as well as to resolve collisions. Finally we present several applications now possible using FIM^{2c}.

nematode *Caenorhabditis elegans* [4]–[6]. The possibility of automated computer-based image acquisition and motion analysis enables high-throughput experiments [7], [8] and complex experimental setups [9]–[11]. In addition, an advanced tool-kit including genetic markers like the green fluorescent protein (GFP) enables sophisticated in vitro and ex vivo analysis [12], [13]. However, none of the systems incorporate precise detections of fluorescent markers like genetic labelling into in vivo whole-body imaging and tracking.

A. Contributions and Organisation of This Paper

1) *Contributions*: Here we introduce a novel multi-purpose imaging system that advances the FIM system [14] by utilizing frustrated total internal reflection of different wavelengths and is called FIM^{2c}. By this FIM^{2c} enables the simultaneous detection of freely crawling animals and fluorescent markers like GFP or fluorescent tracers. In particular, we elaborate the optical path and physical principle of FIM and FIM^{2c} in detail which was not done in the previous publications focussing on the biological applicability rather than technical aspects.

By imaging light reflections (indicating the animals posture and motion) and light emission (e.g. induced by GFP exhibition or markers of fluorescein) we tested a variety of different experimental approaches. For example, FIM^{2c} can be used to image GFP positive cells / tissues / animals during free crawling experiments and is applicable for a variety of different

model organisms like *Drosophila melanogaster* larvae or *C. elegans*. Also food can be labelled by UV excitable markers to image food intake in multi-target tracking approaches for example. In addition, optogenetics can be employed directly into large scale behavioural experiments. Furthermore, it can be used to resolve colliding larvae to study social interaction behaviour. Up to now there is no tracking approach available to precisely and reliably resolve the posture and motion during animal-animal contacts. To demonstrate the capabilities of FIM^{2c} and to make our results available for the community, we set-up a comprehensive database including images and tracked larval models of more than 1,300 resolved collisions necessary to implement and test marker-less collision resolution strategies.

The overall system lay-out is summarized in Figure 1. All aspects including the software, construction instructions and the collision database will be made available for the community.

2) *Organisation*: This paper is structured as follows. In Section II-A the hardware design of FIM^{2c} is described. Subsequently, the physical principle with special attention to the optical path and resultant reflections and emission is given in Section II-B. The algorithmic steps necessary to image and track using FIM^{2c} imaging are explained in Section II-C, namely the integration of the stereo-camera system to image reflections and emissions (Section II-C1), adjustments made in FIMTrack to process FIM^{2c} images (Section II-C2) and how collisions can be resolved (Section II-C3).

In Section III-A the contrast and overall image quality is examined. A variety of different applications is given in Section III-B (cf. Figure 1). A final discussion and conclusion is given in Section IV and Section V.

B. Related Work

The quantitative analysis of behavioural traits includes two challenging tasks: the image acquisition and the subsequent locomotion feature extraction (i.e. tracking). The related work of both tasks is briefly examined in the following sections. Furthermore, we review the current state-of-the-art techniques related to the applications described in Section III-B.

1) *Image Acquisition Techniques*: Most frequently, camera-based setups combined with appropriate illumination are used to acquire images. Both, incident and transmitted light is employed in behavioural experiments, so that either light reflections [15] or absorptions [16] are recorded.

Many animals require very specific conditions during the experiments aggravating the image acquisition. For example, *Drosophila* larvae and *C. elegans* require a moist surface (generally agar [7], [17]). Unfortunately, the moist surface causes light and object reflections resulting in ambiguities during animal segmentation. Furthermore, a poor contrast between semi-translucent animals and the background complicates the most essential object detection steps [18]. Several image enhancement strategies ranging from colourising the animals [18] or the agar [19] to adjusting the illumination [20], [21] have been introduced.

As an alternative to camera-based recording, lens-less optical imaging and image-sensor-less on-chip acquisition techniques are used to extract posture and motion features. The on-chip optical imaging techniques utilize a complementary metal oxide semiconductor (CMOS) or charge couple device (CCD) sensor chip to measure the shadow of the animals on the image sensor (optofluidic microscope) [22], [23]. Instead of using image sensors, orthogonally arranged microelectrodes are used to measure the resistance change that indicates the presence of the animal's body [24].

To study the locomotor behaviour in more detail microscopes are used to visualize organs or specific tissues at high spatial resolution. For example, confocal microscopy was used to visualize the contraction wave progression [25] or segmental muscles of *Drosophila* larvae [1].

2) *Tracking Approaches*: After imaging tracking algorithms are utilized to extract locomotion features [26]. Obviously both, the total number of extractable features as well as the precision strongly depends on the measurement quality. Several tracking programs have been introduced, including commercially available software (e.g. EthoVision [27]) and custom solutions (e.g. MWT [7], MAGAT [21], SOS [28]).

The major problem of all tracking approaches is the inability to resolve colliding animals. Considering animal-animal contacts, no precise posture and motion quantification is possible any more since individual contours merge into single blobs. As a consequence, current solutions reject these measurements and reinitialize the tracking after the collision has terminated so that the animals have new identities and trajectories are fragmented.

To overcome the problem of losing identities the idTracker uses correlograms to generate a rotational and translational invariant finger prints of the animals [29]. Since correlograms are based on contrast informations, these features cannot be applied to animals like *Drosophila* larvae. Furthermore, no posture and locomotion features can be extracted during the collisions.

In a different approach, the condensation algorithm is used to quantify multiple *C. elegans* [4]. Collisions are addressed by modelling the animal's posture and motion in ambiguous situations. Others tried to resolve colliding animals using weakly supervised structured leaning [30]. However, a precise posture extraction of touching or overlapping animals is still not possible.

3) *Specific Tracking Applications*: All above mentioned setups neither facilitate precise labelling of internal organs nor allow to image gene expression patterns during high-throughput open-field locomotion experiments. However, some approaches combining fluorescent markers and free locomotion either use high magnification and a movable stage to image a single animal [31] or quantify the fluorescent intensity of several animals moving in 3D (adult fruit flies [32], [33]). As a consequence, precise labelling of inner organs in high-throughput experiments is still impossible.

Locomotion phenotypes of experimental animals (i.e. tester) must be analysed in comparison to wild type behaviour (i.e. control animals), thus experiments require extensive controls. Due to the same optical appearance of tester and control

animals, imaging must be done separately. However, due to changing conditions in consecutive trials, the behavioural output might change drastically so that rearing the animals in the same vials and tracking control and tester simultaneously is desirable for comparability. To distinguish sub-populations of walking adult fruit flies, fluorescence behavioural imaging (FBI) has been introduced [34]. Even though the tracking arena was comparatively small (80mm × 20mm), only small fluorescent blobs can be recognized in the fluorescence image.

Optogenetic tools have been used to study how specific cell types contribute to neural functioning [35]. For example, an optogenetic system has been introduced recently to examine how neurons contribute to transform sensory inputs into motor outputs [36].

4) *FIM Imaging and FIMTrack*: We recently introduced FIM (FTIR-based Imaging Method) which utilises frustrated total internal reflection (FTIR) to measure the contact surface of the animals on the tracking stage or the substrate resulting in a superb foreground background contrast [14]. Because of the high contrast, even subtle changes in light intensity can be measured, so that internal structures can be visualized without using microscope magnification [37]. This can be used to determine the orientation of *Drosophila* larvae in our associated FIMTrack software [38].

It has been shown that FIM and FIMTrack are capable to extract posture and locomotion features with very high sensitivity so that even subtle phenotypes can be quantified in high-throughput experiments [14], [37]. However it does not incorporate the rich tool-kit of genetics including fluorescent markers and optogenetics into in vivo whole-body imaging and tracking.

II. METHODS

Both, FIM and FIM^{2c} differ from other imaging techniques by relying on the physical principle of frustrated total internal reflection. By this, an overall black background can be established and the illumination of the animals is induced by their contact with the surface: Rays of light are scattered by the animals and the reflection is no longer total at these interfaces. This indirect illumination technique can be used for all wavelengths.

The general biological usability as well as the basic principle of FIM are demonstrated elsewhere [14], [38]. A precise description of the technical and physical aspects in general was however not elaborated. In addition, neither fluorescent labelling nor optogenetics were feasible in the previous system. This paper focuses on the multi-wavelength extension FIM^{2c} and supplies the physical and technical details of the light propagation and how frustrated total internal reflection is used to capture both, light reflections and emission. Furthermore, necessary algorithmic extensions are presented to facilitate a variety of different applications.

A. FIM^{2c} Hardware Overview

To image the posture and motion of the animals as well as fluorescent markers two different types of LEDs are mounted at the edge of the tracking stage, namely infrared (IR) LEDs

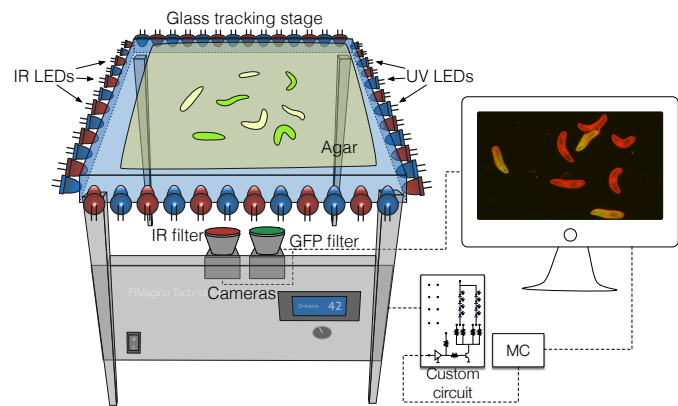


Fig. 2. Overview of FIM^{2c} hardware design. Green larvae indicate labelled animals and yellow larvae indicate non-labelled animals. All necessary components are indicated.

(HP HSDL-4230) and ultraviolet (UV) LEDs (LC503FBL1-15P-A3; Figure 2). The IR and UV light sources have a dominant wavelength of 875nm and 470nm respectively. We used custom circuits and micro controllers (MC) to regulate the illumination intensity equivalent to the single-colour FIM setup [14].

In contrast to FIM, a stereo-camera system (two Basler acA2040-25gm cameras) equipped with 35mm objectives (KOWA LM35HC) is used for imaging. Besides the IR long pass filter with a cut-on wavelength of 825nm (Schneider Kreuznach IF093), a custom GFP bandpass filter is mounted to the so-called GFP camera (bandpass $526 \pm 20\text{nm}$; AHF BrightLine HC 536/40). Both, the cameras and the micro controllers are connected to the same computer to control camera settings and illumination intensity in a closed loop. To provide a moist surface, an agar layer is placed on the glass so that the animals can crawl freely on this layer (0.8% food grade agar boiled in deionized ultra pure water; cf. Figure 2).

B. FTIR in the FIM^{2c} System

The FIM^{2c} system utilized total internal reflection (TIR) to flood the tracking stage with IR and UV light [39]. The posture of the animals is imaged using the so-called IR camera based on reflected IR light caused by frustrated total internal reflection (i.e. touches on the surface; compare to [14]) whereas the fluorescent markers cause green light emission captured by the GFP camera. Note that the general feasibility as well as the biological applicability are given in [14], [38] without elaborating the physical details. Therefore, the light propagation as well as the reflection and emission is described in the following sections.

1) *Light Propagation and Total Internal Reflection*: To monitor freely crawling animals using FIM^{2c} they are placed on a thin agar layer (2mm height). The agar layer is located on the acrylic glass plate which is flooded with IR and UV light. Three media need to be examined in terms of optical properties to describe the light propagation: air, acrylic glass and agar.

The refractive indices of air and glass can be approximated by $n_{\text{air}} = 1.00$ and $n_{\text{acrylic}} = 1.49$ respectively. In contrast,

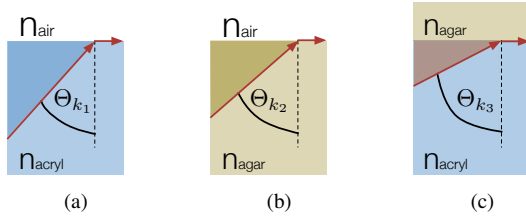


Fig. 3. Different critical angles for TIR. Given the refractive indices $n_{\text{air}} = 1.00$ for air, $n_{\text{acrylic}} = 1.49$ for acrylic glass and $n_{\text{agar}} = 1.33$ for agar, the resultant critical angles are (a) $\Theta_{k_1} = 42.16^\circ$ for the acrylic glass / air boundary, (b) $\Theta_{k_2} = 48.75^\circ$ for the agar / air boundary and (c) $\Theta_{k_3} = 63.20^\circ$ for the acrylic glass / agar boundary. Coloured areas above the critical angles indicate intervals in which the light is reflected totally.

the refractive index of agar varies considering different agar / water concentrations. Using an agar concentration of 0.8% the refractive index can be assumed to be similar to water leading to $n_{\text{agar}} = 1.33$ [40].

Next, three boundaries and their critical angles Θ_k need to be examined in order to analyse the total internal reflection:

- Acrylic glass \rightarrow air boundary (with its critical angle $\Theta_{k_1} = 42.16^\circ$)
- Agar \rightarrow air boundary (with its critical angle $\Theta_{k_2} = 48.75^\circ$)
- Acrylic glass \rightarrow agar boundary (with its critical angle $\Theta_{k_3} = 63.20^\circ$)

The corresponding critical angles are illustrated in Figure 3. All critical angles are calculated based on Snell's law $n_i \sin(\Theta_k) = n_j \sin(\gamma)$ assuming a refraction $\gamma = 90^\circ$ and $n_i > n_j$ [39].

These properties can be used to describe the light propagation: Rays of light enter the acrylic glass at the edges of the tracking stage (Figure 5). Due to the differences in the refractive indices of acrylic glass and air ($n_{\text{acryl}} > n_{\text{air}}$), light with an incidence angle Θ_1 above the critical angle $\Theta_{k_1} = 42.16^\circ$ is completely reflected at the glass / air boundary (i.e. total internal reflection; cf. Figure 3a). Light with an angle of incidence in-between ($\Theta_{k_1}, \Theta_{k_3}$) (i.e. $(42.16^\circ, 63.20^\circ)$) enters the agar. Note that the left boundary guarantees total internal reflection at the glass / air interface and the right boundary enables a transmission from glass to agar (cf. Figure 3c).

During this transition from glass to agar the rays refract away from the perpendicular since $n_{\text{agar}} < n_{\text{acryl}}$. Their new direction in the agar can be calculated by $\gamma = \arcsin\left(\frac{n_{\text{agar}}}{n_{\text{acryl}}} \cdot \sin(\Theta_1)\right)$. As long as $\gamma > \Theta_{k_2} = 48.75^\circ$, the light is reflected at the agar / air boundary (cf. Figure 3b) and thus trapped inside the glass / agar double layer. Possible refractions γ for $\Theta_1 \in (42.16^\circ, 63.20^\circ)$ and corresponding critical angles Θ_{k_2} are plotted in Figure 4. Obviously, almost all rays of light, which are completely reflected at the acrylic glass / air boundary (i.e. $\Theta_1 > \Theta_{k_1}$) and refracted during the glass / agar transition are also completely reflected at the subsequent agar / air boundary (i.e. $\gamma > \Theta_{k_2}$).

2) *Imaging Reflection and Emission*: If a larva touches the agar light of both wavelengths is no longer reflected totally and can pass through the larva / agar interface so that it enters the semi-transparent animal. The larval tissues scatter the IR

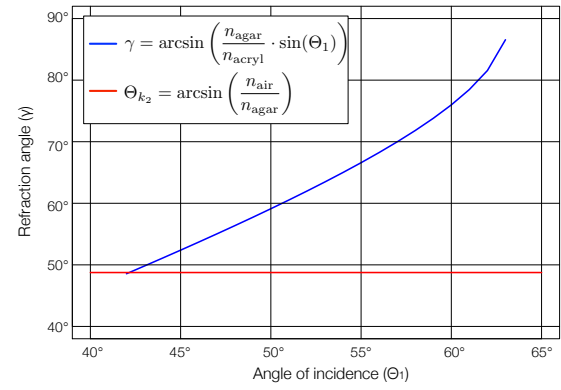


Fig. 4. Refraction γ during transition from acrylic glass to agar. γ is plotted for all possible angles of incidence $\Theta_1 \in (42.16^\circ, 63.20^\circ)$. All angles above Θ_{k_2} (red line) are completely reflected at the agar / air boundary.

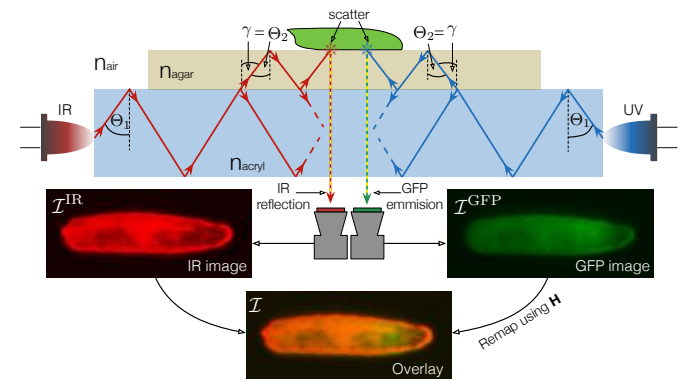


Fig. 5. FTIR in the FIM^{2c} setup. Frustrated rays of light passing through all layers are highlighted by arrows dashed in yellow. Note that UV light (blue arrow) excites GFP so that it emits green light (green arrow) which is in turn detected by the GFP camera. The larva in the resultant images expresses *daughterless Gal4* so that the whole animal is labelled.

light so that it propagates in all directions (Figure 5). All reflected rays with angles below the critical angles Θ_{k_1} , Θ_{k_2} and Θ_{k_3} are not reflected totally anymore. The light is said to be frustrated (FTIR) and can pass through the layers so that it can be captured from underneath. Given GFP expressing larvae, the UV light enters the animals equivalent to the IR light. However, this time the green fluorescent protein (GFP) is excited by the UV light and emits 509nm (green) light, which is detected by the GFP camera. The light propagation as well as the reflection and emission is illustrated in Figure 5.

In summary, the following properties must be satisfied considering the optical properties of the materials used in FIM^{2c}:

- 1) $n_{\text{air}} < n_{\text{acryl}}$ to ensure total internal reflection at the acrylic glass / air boundary
- 2) $n_{\text{air}} < n_{\text{agar}}$ to ensure total internal reflection at the agar / air boundary
- 3) Larvae must scatter light so that the total internal reflection is frustrated and IR light can pass through all layers
- 4) UV light must illuminate the GFP-tagged larvae to exhibit bright green fluorescence

As shown in Figure 7 the first two properties provide a dark background whereas the third property guarantees bright larvae. The last property enables imaging of the fluorescent markers.

C. FIM^{2c} Algorithms

In order to use FIM^{2c} in a variety of different applications several algorithmic adjustments need to be employed. Firstly overlays must be generated using the stereo-camera system and secondly the tracker must be adjusted to integrate GFP emissions. Finally we demonstrate how collisions can be resolved using tagged and non-tagged animals.

1) *Stereo-Camera Imaging*: Considering two images \mathcal{I}^{IR} and \mathcal{I}^{GFP} from the IR and GFP camera respectively. Let $p_i^{\text{IR}} = (x_i^{\text{IR}}, y_i^{\text{IR}})$ be a point in \mathcal{I}^{IR} and $p_i^{\text{GFP}} = (x_i^{\text{GFP}}, y_i^{\text{GFP}})$ be a point in \mathcal{I}^{GFP} . Then the source image \mathcal{I}^{GFP} is mapped to the destination image \mathcal{I}^{IR} by

$$s_i \cdot \begin{pmatrix} x_i^{\text{IR}} \\ y_i^{\text{IR}} \\ 1 \end{pmatrix} = \mathbf{H} \cdot \begin{pmatrix} x_i^{\text{GFP}} \\ y_i^{\text{GFP}} \\ 1 \end{pmatrix}$$

The matrix $\mathbf{H} \in \mathbb{R}^{3 \times 3}$ facilitates the perspective transformation between the GFP camera and the IR camera and is called homography (s_i is a scale factor). To determine the homography, several unique calibration patterns are placed on the agar. The SURF feature detector [41] is used to find feature points on the calibration pattern in both views. Subsequently, SURF descriptors are calculated.

Let $\mathbf{v}_i^{\text{IR}}, i = 1, \dots, N$ and $\mathbf{v}_j^{\text{GFP}}, j = 1, \dots, M$ be the descriptor vectors corresponding to points p_i^{IR} in the IR and p_j^{GFP} in the GFP image respectively. To match interest points between the views the FLANN matcher [42] is utilized resulting in pairs $\mathbf{m}_k = (\mathbf{v}_i^{\text{IR}}, \mathbf{v}_j^{\text{GFP}}), k = 1, \dots, K$. For the homography calculation only matches below a given distance $\varepsilon = 3 \cdot \min_{k=1, \dots, K}(\text{dist}(\mathbf{m}_k))$ are considered, whereby $\min_{k=1, \dots, K}(\text{dist}(\mathbf{m}_k))$ is the minimal distance found for all matches. Let

$$M^* = \{(p_i^{\text{IR}}, p_j^{\text{GFP}}) \mid \forall (p_i^{\text{IR}}, p_j^{\text{GFP}}, \mathbf{m}_k) : \text{dist}(\mathbf{m}_k) < \varepsilon\}$$

be the set containing all pairs of points with a distance below ε . The homography \mathbf{H} is then calculated based on M^* using the RANSAC paradigm [43] by minimizing the back-projection error

$$\sum_i \left(x_i^{\text{IR}} - \frac{h_{11}x_i^{\text{GFP}} + h_{12}y_i^{\text{GFP}} + h_{13}}{h_{31}x_i^{\text{GFP}} + h_{32}y_i^{\text{GFP}} + h_{33}} \right)^2 + \left(y_i^{\text{IR}} - \frac{h_{21}x_i^{\text{GFP}} + h_{22}y_i^{\text{GFP}} + h_{23}}{h_{31}x_i^{\text{GFP}} + h_{32}y_i^{\text{GFP}} + h_{33}} \right)^2$$

The resultant matrix \mathbf{H} is applied to the GFP image \mathcal{I}^{GFP} . Finally, the transformed image and the IR image \mathcal{I}^{IR} are stored within the same multi-channel image \mathcal{I} so that \mathcal{I}^{IR} is accessible via the red channel and \mathcal{I}^{GFP} is accessible via the green channel resulting in an overlay image (Figure 5).

2) *2-Color Detection*: The tracking algorithm described in [38] is adjusted to employ FIM^{2c} images. Let $\mathcal{I}_t^{\text{IR}}$ and $\mathcal{I}_t^{\text{GFP}}$ be the red and green channel of the overlay image \mathcal{I}_t at time t . Considering N animals imaged including n^{IR} non-GFP labelled animals and n^{GFP} animals expressing GFP ($n^{\text{IR}} + n^{\text{GFP}} = N$). As mentioned above, all N animals can be detected in $\mathcal{I}_t^{\text{IR}}$, whereas $\mathcal{I}_t^{\text{GFP}}$ includes only the GFP extinctions of n^{GFP} animals. Thus, $\mathcal{I}_t^{\text{IR}}$ is used to identify the larvae and to calculate all locomotion related features.

Using the contours C_t from $\mathcal{I}_t^{\text{IR}}$, the mean green intensities \bar{g}_t^i can be calculated by masking the remapped $\mathcal{I}_t^{\text{GFP}}$ with contours $c_t^i \in C_t$ and calculating the intensity averages inside these masks. Given the sorted set of mean green value intensities of N_t animals $G_t = \{\bar{g}_t^i\} (i = 1, \dots, N_t)$, a larva is a GFP larva if $\bar{g}_t^i > \tau^{\text{GFP}}$:

$$b^{\text{GFP}} = \begin{cases} 1 & \text{if } \bar{g}_t^i > \tau^{\text{GFP}} \\ 0 & \text{otherwise} \end{cases} \quad (1)$$

This threshold is calculated automatically by determining

$$\tau^{\text{GFP}} = \frac{\bar{g}_t^{i^*} + \bar{g}_t^{i^*-1}}{2} \quad (2)$$

where $(i^* - 1, i^*)$ indicate consecutive indices of mean green intensities with highest positive slope:

$$i^* = \arg \max_{\bar{g}_t^{i-1}, \bar{g}_t^i \in G_t} (\bar{g}_t^i - \bar{g}_t^{i-1})$$

3) *Resolving Collisions*: The following conditions must be satisfied in order to resolve collisions within the FIM^{2c} system:

- 1) Only two larvae participate within a collision
- 2) One of the two animal must express GFP exclusively so that the whole shape of the larvae is detectable in \mathcal{I}^{GFP}

The first condition can be verified using the binary indicator described in Equation 1. The second condition can be achieved by using appropriate genetic constructs like GFP labelled *daughterless Gal4* animals (*daGal4*; cf. Figure 10).

Let the contour of larva i at time t be c_t^i . The area of a single contour $A(c_t^i)$ is restricted by λ_{max} , so that all contours $A(c_t^i) \geq \lambda_{\text{max}} (t > 1)$ indicate collisions. All larvae l_{t-1}^i from time $t - 1$ having at least one point within the collision contour c_t^i at time t are identified as collision participants. Valid points of l_{t-1}^i are the spine points including the head and tail $\mathbf{h}, \mathbf{s}_1, \dots, \mathbf{s}_{L-2}, \mathbf{t}$ and the centre of mass \mathbf{m} . Collisions are assumed to be resolvable as long as only two larvae are involved in the collision and one of the two larvae is a GFP larva ($b^{\text{GFP}} = \text{true}$; Equation 1). The other larva have to be a non-GFP expressing animal ($b^{\text{GFP}} = \text{false}$). All collisions that do not satisfy both conditions are rejected.

Remaining resolvable collision contours c_t^i are processed in a subsequent collision resolution algorithm (Figure 6). After splitting the 2-colour image into the red and green channel \mathcal{I}^{IR} and \mathcal{I}^{GFP} the algorithm uses \mathcal{I}^{GFP} to segment the contour of the GFP expressing animal. The segmentation threshold $\tau_{\text{col}}^{\text{GFP}}$ is determined by analysing the green value distribution within the collision contour.

In theory, both larvae cover approximately the same area so that 50% of the foreground pixels belong to the GFP larvae and the remaining 50% belong to the non-tagged larvae. Therefore,

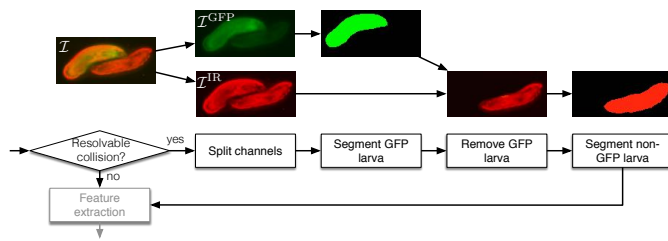


Fig. 6. Overview of the collision resolution algorithm. The collision image is separated into the IR and GFP channel, the green larva is segmented in the GFP image and removed from the IR image. The remaining pixels in \mathcal{I}^{IR} belong to the non-tagged animal.

the mean intensity μ^{green} is sufficient to separate only the GFP larvae via thresholding ($\tau_{\text{col}}^{\text{GFP}} = \mu^{\text{green}}$): All pixels within the collision contour c_t^i which are above $\tau_{\text{col}}^{\text{GFP}}$ are assumed to belong to the GFP larvae and removed from the infrared channel. All remaining pixels in \mathcal{I}^{IR} belong to the non-labelled animal. To smooth the resultant contours a morphological *open-operation* with an elliptical kernel is used. Afterwards, these contours can be utilized to calculate all features and tracking is done as described in [14], [38].

D. Fly Handling and Animal Preparation

For the experiments wandering third instar stages of *Drosophila melanogaster* larvae have been collected from standard fly vials. Animals have been reared in standard conditions at 25°C and 65% humidity. A constant dark night cycle was applied.

For all experiments expression of fluorescent proteins was achieved using the binary Gal4/UAS expression system [44]. For the experiment explained in Section III-B1 larvae of the w^{1118} strain were used together with larvae expressing GFP ubiquitously of the genotype [*da-Gal4*, UAS-GFP].

For experiments described in Section III-B2 we used flies with the genotype [*da-Gal4*, UAS-GFP] GFP as well as [*en-Gal4*, UAS-GFP] or [*nrv2-Gal4*, UAS-GFP]. The *engrailed* (*en*) promoter directs expression in cells at the distal border of each segment. The *nervana2* (*nrv2*) promoter directs expression in a specific subset of glial cells, including three wrapping glial cells in each abdominal nerve. For the experiment given in Section III-B3 larvae were fed with food that contained fluorescein.

For the experiment described in Section III-B4 we used animals with the genotype [*ppk-Gal4*, UAS-ChR2]. Here, expression of *Channel Rhodopsin 2* (*ChR2*) is activated in multi dendritic sensory neurons. *ChR2* can be activated by blue light which leads to the influx of cations, thereby depolarizing and activating the expressing neurons. This results in a profound escape behaviour therefore larvae sweep their heads or start rolling.

For the experiment given in Section III-B5 we used *Caenorhabditis elegans* worms, that have been fed with bacteria expressing GFP.

For the experiment in Section III-B6 we used w^{1118} larvae and [*da-Gal4*, UAS-GFP] larvae. Ubiquitous expression of GFP is critical to define the contours of two larvae in contact.

TABLE I
UV IRRADIATION IN THE FIM^{2c} SYSTEM.

Intensity in %	Irradiation in lux
0	0
12	55
24	111
36	170
48	235
60	300
72	366
84	434
100	528

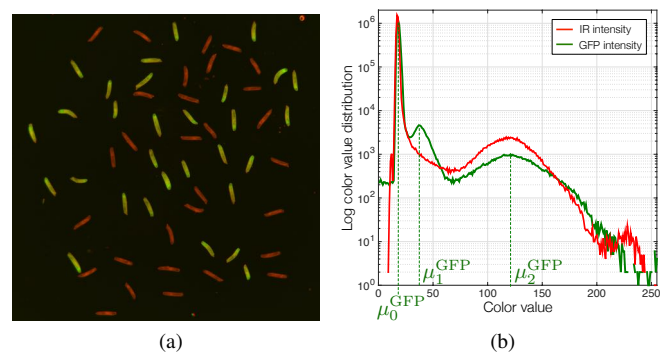


Fig. 7. FIM^{2c} image and corresponding red and green channel histogram. (a) 2-colour image at 55% illumination intensity. (b) The red channel is a bimodal distribution, whereas the green channel consists of three Gaussian distributions. Mean green intensities for the background μ_0^{GFP} , the non-labelled animals μ_1^{GFP} and the GFP expressing animals μ_2^{GFP} are indicated.

III. RESULTS

The results are structured as follows: First the overall contrast of the FIM^{2c} imaging system is analysed quantitatively. Subsequently, a variety of different applications are examined and we present a database of resolved colliding larvae.

A. Overall Contrast

To analyse the UV light intensity, we measured the brightness using a photometer. The sensor was inserted into the agar to detect the light. As indicated by Table I, the UV irradiation increases linearly with the illumination intensity ranging from 0 to more than 500 lux.

To quantify the contrast in the 2-colour images several dead labelled and non-labelled animals are placed on the tracking stage (Figure 7a). Note that some of the larvae are genetically engineered to ubiquitously express GFP (i.e. *daGal4*) so that a strong green light emission is guaranteed [45]. Both, the IR and UV illumination intensity were set to 55%.

In Figure 7b the histogram of \mathcal{I}^{IR} is given in red and the histogram of \mathcal{I}^{GFP} is given in green. Only animals touching the surface can be measured in \mathcal{I}^{IR} so that the distribution is bimodal: N animals appear as bright objects (right Gaussian) within the almost black background (left Gaussian). In \mathcal{I}^{GFP} , the distribution consists of three Gaussian distributions covering the background (μ_0^{GFP}), the non-tagged

larvae (μ_1^{GFP}) and the GFP larvae (μ_2^{GFP}) respectively (green line in Figure 7). Thus both \mathcal{I}^{IR} and \mathcal{I}^{GFP} can be segmented using thresholding operations given a threshold τ^{IR} to segment the animals in the IR image and a threshold τ^{GFP} to differentiate GFP larvae from non-labelled larvae in the GFP image (compare to Equation 2).

Since the IR and the UV intensity can be set separately, optimal illumination for segmentation might require a specific combination of these two values. For example, the IR filter might be sufficient to block visible light, but less effective in the UV light spectrum. In addition, the autofluorescence of the larvae might cause interferences. Thus, the mutual influence of both illumination intensities is analysed based on the Weber contrast to quantify the luminance difference between the background and foreground:

$$W_c(i, j) = \frac{\mu_1(i, j) - \mu_0(i, j)}{\mu_0(i, j)}$$

where $\mu_1(i, j)$ and $\mu_0(i, j)$ represent the mean foreground and background intensity for a given IR irradiation i and UV irradiation j .

In \mathcal{I}^{GFP} two different object brightnesses can be determined, one for the non-labelled and one for the labelled animals. Even if the animals do not express GFP, slight auto-fluorescent light emissions are measured in the GFP image (Figure 7 μ_1^{GFP} and μ_2^{GFP}). Thus, two foreground masks are calculated for \mathcal{I}^{GFP} : $\mathcal{M}_{labelled}^{GFP}(j)$ to segment GFP labelled animals only and $\mathcal{M}_{all}^{GFP}(j)$ to segment all animals.

Based on these masks the Weber contrast of the labelled and all animals is calculated and plotted for all possible IR and UV intensities (Figure 8). The overall contrast in \mathcal{I}^{GFP} is only influenced by the UV illumination intensity since no changes can be recognized for different IR intensities. Thus, the GFP filter is sufficient to block reflected IR light. The foreground variance is increased in case of a $\mathcal{M}_{all}^{GFP}(j)$ -based segmentation since GFP fluorescence and auto-fluorescence are within the foreground distribution. As a consequence, the overall contrast is reduced (compare to *all larvae* surface in Figure 8).

In contrast, a segmentation based on $\mathcal{M}_{labelled}^{GFP}(j)$ leads to an even higher contrast than the highest contrast in \mathcal{I}^{IR} (data not shown). The reason for this can be found in the different origins of the detected light: The detections (i.e. foreground) measured in \mathcal{I}^{IR} are caused by frustrated IR light, whereas the foreground intensity measured in \mathcal{I}^{GFP} given $\mathcal{M}_{labelled}^{GFP}(j)$ is based on the GFP excitation. Considering the strong GFP expression of *daGal4* larvae, a comparatively strong signal is detected in \mathcal{I}^{GFP} so that the overall contrast is very high. Therefore, low UV irradiation is sufficient to induce GFP excitations and thus determine GFP expressing animals. The brightness and contrast of the infrared light is discussed elsewhere [14].

B. FIM^{2c} Applications

In this section several applications of this multi-purpose system are introduced.

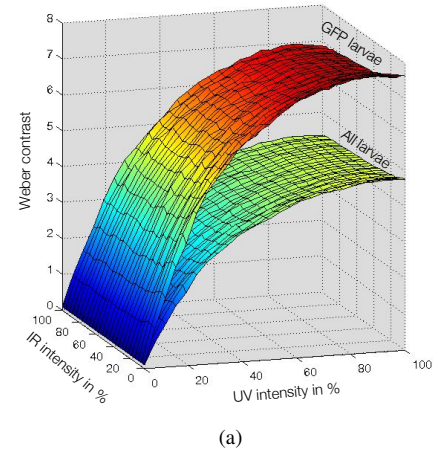


Fig. 8. (a) Weber contrast of \mathcal{I}^{GFP} measured for altering IR and the UV irradiation. The *GFP larvae* surface indicates the contrast calculated only for the GFP labelled larvae and the *All larvae* surface indicates the contrast for all larvae (including the non-labelled larvae). (b) Green channel (i.e. \mathcal{I}^{GFP}) of three GFP expressing *daGal4* larvae and three wild-type larvae. Note the autofluorescence of the non-labelled animals.

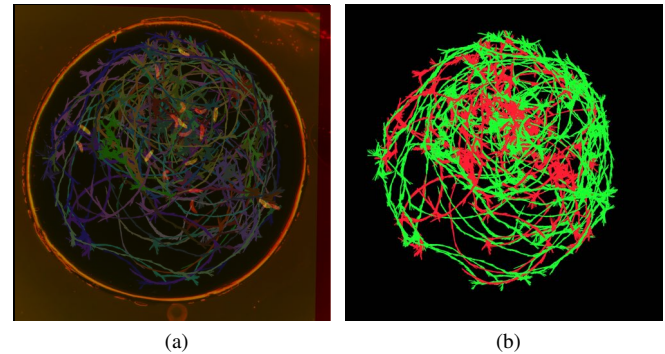


Fig. 9. Tracking two genotypes simultaneously. (a) Overlay of the image captured by FIM^{2c} and the resultant locomotion trajectories. (b) Resultant trajectories assigned to the two genotypes. A circular salt barrier was used to prevent the larvae from exiting the field-of-view.

1) *Imaging of Two Genotypes Simultaneously*: Usually, the behavioural phenotype of a specific genetically manipulated animal (i.e. tester) is compared to control animals (e.g. wild type animals). Due to the same optical appearance of control and tester animals imaging must be done separately. Unfortunately, the behavioural output of the animals can change dramatically given different environmental conditions like humidity, temperature or time of day.

Using FIM^{2c} control and tester that originate from the same culture vial can be imaged together using genetic engineering. In Figure 9a an overlay image of genetically labelled and control animals with the resultant trajectories is given. Again the green larvae express the fluorescent protein GFP (*daGal4*; called GFP larvae). The subdivision into GFP and non-GFP animals is done using Equation 1. Since control and experimental larvae are now distinguishable, they can be imaged

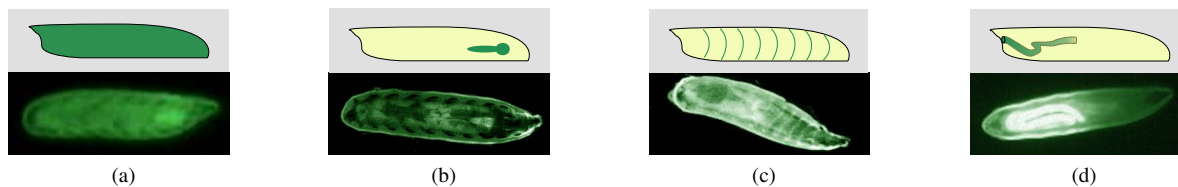


Fig. 10. Internal organs can be labelled by directed expression of GFP: (a) *daGal4* (all cells), (b) *nrv2Gal4* (central nervous system) and (c) *enGal4* (larval segments). (d) Fluorescein fed larva. Note that the gut is glowing. Only I^{GFP} is given.

under the same conditions.

Calculated trajectories are given in Figure 9b. GFP larvae trajectories are highlighted in green, non-tagged animal tracks are given in red.

2) *Labelling Specific Tissues*: Genetic constructs can be used to label internal structures of *Drosophila* larvae and to visualize gene expression. For example, GFP can be expressed in different tissues like the nervous system using the Gal4 system. By *daughterless Gal4 (daGal4)*, all cells can be labelled by GFP emission so that the whole animal is visible in the GFP image (Figure 10a) [45]. Furthermore, we utilized *nervana 2-Gal4* to express GFP in a small subset of glial cells. In the peripheral nervous system (PNS), only three wrapping glial cells express *nervana 2-Gal4* in every abdominal peripheral nerve 14,15 which can be detected using *FIM^{2c}* imaging highlighting the sensitivity (Figure 10b) [46]. *engrailed Gal4 (enGal4)* can be used to visualize the boundary in the larval body segment (Figure 10c) [47].

All images are recorded using conventional GigE cameras which are equipped with standard optics and the GFP filter described above. Thus, no microscope-based magnification is necessary to visualize genetically labelled internal tissues in large-scale experiments. It should be noted that only the green channel is shown in Figure 10. These gene expression patterns can be used in combination with locomotion features extracted by the FIM tracking software.

3) *Fluorescent Tracers*: In other experiments the foraging behaviour of *Drosophila* larvae can be examined based on their locomotion trails [48]. If a precise measurement of food-intake is necessary, measurements are currently done using adult flies mainly [48]–[50].

Besides genetic constructs used above, fluorescent markers can be utilized in the *FIM^{2c}* system to label specific tissues or organs. A proof-of-principle example is given in Figure 10d in which a larva was fed with fluorescein containing food. The midgut of the animal is clearly visible. This suggests, that *FIM^{2c}* can be used in feeding behaviour studies and is expandable for foraging experiments.

4) *Optogenetics in FIM^{2c}*: In optogenetics, light of a particular wavelength can be used to control the activity of individual cells (e.g. neurons) in moving animals [51]. This is achieved by integrating light-sensitive proteins like channelrhodopsin or halorhodopsin into the neuronal plasma membrane. For example, channelrhodopsin (i.e. *ChR2*) is a light-gated ion channel which opens upon blue light irradiation (~ 480 nm) so that Na^+ ions can pass, leading to a depolarization of the membrane potential, which in turn causes action potentials. It has been shown that *ChR2* is capable to

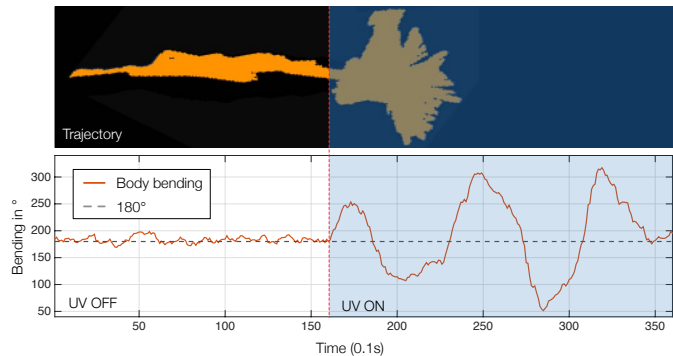


Fig. 11. Optogenetic in *FIM^{2c}*. Top: Track of a single optogenetically modified larvae before and after the UV light was turned on. Bottom: Body bending of the larvae shown in the trajectory before and after UV light has been turned on (180° indicate no bending). Note the strong nociceptive bending after UV light has been activated.

cause light-induced action potentials in the motor system of *Drosophila* [52]. In the past, *ChR2* was used to trigger the specific rolling behaviour [53].

The *FIM^{2c}* setup is equipped with LEDs emitting ~ 470 nm UV light. We tested the optogenetic capabilities in terms of triggering the rolling response using the UV light. This was done by expressing *ChR2* specifically in neurons that trigger this response to nociception. The animals were placed on the tracking stage which was not illuminated by UV light. After 16 seconds we activated the UV LEDs (100% illumination leading to ~ 528 lux irradiation). The resultant trajectory of a single larva is given in Figure 11 (top). The animal contracted its body immediately after the UV light was turned on. In fact, regular forward locomotion was almost impossible during the first 20 seconds after light stimulation which is not the case in control animals.

The contraction resulting in left and right body bendings can be quantified by FIMTrack using the bending angle γ_{bend} [38]. In Figure 11 (bottom) the bending of the larva's trajectory given in Figure 11 top is plotted over time. Up to second 16 the animal was crawling forward with almost no body bending ($\gamma_{\text{bend}} \approx 180^\circ$; compare to dashed line in Figure 11 bottom). After the light has been turned on, strong bending to the left and right can be recognized.

We observed a similar rolling behaviour phenotype as reported in [53]. The animals turned them-self around their main axis, however they did not perform complete 360° rolls frequently. Instead, strong alternating body bends and rotations of approximately $\pm 150^\circ$ were observed during UV irradiation. In summary, this demonstrates that *FIM^{2c}* can be

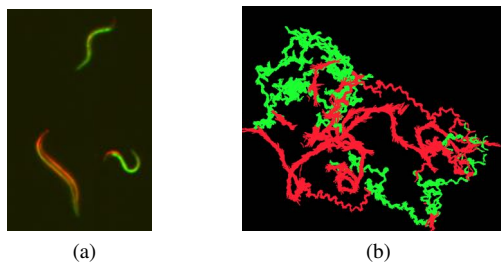


Fig. 12. Analysis of *C. elegans* with FIM^{2c}. (a) 3 worms are shown; two of them are expressing GFP. Inner body structures like the Pharynx are recognizable. (b) Worm trajectories. *C. elegans* worms can be tracked with the same accuracy as *Drosophila* larvae. The green worms are distinguishable from red worms (compare to Figure 9).

used to induce optogenetic responses based on proteins like channelrhodopsin.

Note that both light sources for imaging and optogenetic activation are mounted at the edges of the tracking stage. Since the cameras are recording from below all stimulations (e.g. heat) applicable from above can still be integrated (for examples see [14]). Thus, optogenetic studies can be facilitated within FIM^{2c} without any structural or experimental restrictions.

5) *Imaging & Tracking Caenorhabditis elegans*: Besides applications for *Drosophila* larvae, FIM and FIMTrack are also capable to image and track *C. elegans* worms (Figure 12a) which are smaller than *Drosophila* larvae (0.3–1mm compared to 1–5mm). A whole suit of behavioural experiments has been developed for *C. elegans* worms (M. Kiel, in preparation). Here we show, that expression of GFP can also be imaged in *C. elegans*. Figure 12b shows the possibility to apply FIM^{2c} to *C. elegans* and track two genotypes simultaneously. Not only the GFP expressing worms, but also the distinction of major characteristics like the pharynx or the intestine is easily possible. However, higher magnification is necessary to label and visualize specific tissues. Taken together these results confirm that FIM^{2c} can be applied to different organism even if those organisms are much smaller than *Drosophila* larvae.

6) *Collision Database*: Collisions are a major concern in multi-target tracking since they cause a loss of identity and fragmented trajectories. Furthermore, collisions cause significant behavioural changes after collisions [54].

To resolve collisions and to generate a collision database we placed six *w¹¹¹⁸* larvae together with six *daGal4 UASCD8GFP* larvae on an agar arena (9.5 cm diameter; cf. Figure 9a). We allowed the larvae to crawl freely in the absence of stimuli for 7 minutes. Imaging was done using IR- and UV-light. Only collisions between single GFP expressing and single non GFP expressing animals with no overlays were counted as valid collisions. Valid collisions were inspected manually using the results viewer [38]. Two examples are given in Figure 13. In summary, 55 videos with 4,200 frames each were analysed.

Note that the collision resolution algorithm described above can only be applied to FIM^{2c} images using UV light to exhibit green fluorescence. As a consequence there are two limitations given the FIM^{2c} collision resolution. First, one of the two

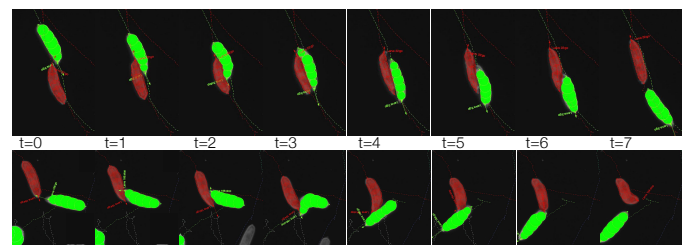


Fig. 13. Two resolved collisions. The GFP expressing larva is given in green and the non-labelled larva is given in red.

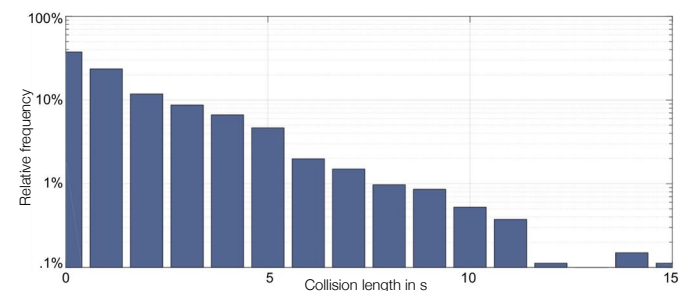


Fig. 14. Distribution of collision lengths in the collision database. Length of each collision is given in seconds (x-axis) and frequencies are logarithmised (y-axis).

colliding animals must express GFP and second, UV-light must be present during recordings. Even though the difference in behaviour with and without our very weak UV illumination was negligible [54] a label-free / UV-free collision resolution algorithm would be desirable.

To provide the ground truth for the resolution of colliding larvae we established a database with more than 1,300 resolved collisions (supplementary database). In the database we kept the collision data for both opponents with a maximum of 50 frames before and after the collision. This results in more than 2,800 datasets. Larval collisions can be classified based on the duration of larval contacts. 25% of the collisions are very short and last less than 0.5 seconds whereas the other collisions last longer (Figure 14). Compared to the existing database presented in [30] which is used to keep track of the identity before and after the collision, our database includes complete larval models over time including the head and tail position and several spine points. Thus the database presented here serves as a starting point to implement and test restriction-free collision resolution algorithms in the future, necessary for other researchers.

IV. DISCUSSION

Of course, FIM^{2c} offers many other applications. Due to the high contrast even single-cell labelling is possible. Given a higher sensitivity Ca²⁺ imaging might be possible. Stronger illumination will be sufficient to record changes in calcium levels in cells, which are indicated by molecular calcium sensors, that operate yet again by changing green emission intensity. Therefore, specific proteins can be expressed cell type specifically that change their physical properties, when for example calcium levels in the cells change, which is

in neurons a measure for activity. Expressing Ca^{2+} sensors in neuronal circuits and challenging the larvae with sensory input (e.g. odours / heat) will lead to an understanding of the neuronal substrate that is active to compute the information in these stimuli. Thus, the influence of the sensory stimulation on the circuit, the response and the impact on locomotion can be compared. This will greatly advance the elucidation of circuits integrating sensory informations and controlling behaviour output.

Furthermore it should be noted that FIM^{2c} is not limited to IR and UV light. Other and more than two colours can be integrated. In our current system, we are going to combine four different colours, namely IR at 875nm for whole body imaging, yellow at 587nm for mCherry, green at 560nm for dsRed and tdTomato and UV at 470nm for GFP, fluorescein, etc. (number of cameras and filters must be adjusted accordingly). Thus, we will focus our work to further increase the usability of both, the FIM^{2c} hardware (i.e. image acquisition) and software and integrate other applications and model organisms.

V. CONCLUSION

The need for reliable image acquisition techniques for challenging situations like translucent *Drosophila* larvae or small *C. elegans* worms motivated to develop the FIM setup as a versatile imaging technique [14]. To increase the experimental possibilities, we extended the FIM setup to simultaneously image behaviour and fluorescent markers using a two-camera / two-colour construction. This system utilizes frustrated total internal reflection (FTIR) of infrared and ultraviolet light to image the posture, movement and fluorescent marker emissions and is called FIM^{2c}. UV-light can either be used to elicit fluorescent proteins that have been integrated by genetic engineering (e.g. GFP) or other fluorescent substances like fluorescein. Moreover light responsive proteins that can activate neurons can be used to manipulate the animals actively (e.g. *ChR2* in optogenetic approaches).

As a result a variety of different applications can now be implemented. Here we introduced six exemplary applications: imaging two genotypes simultaneously, labelling specific tissues / cells, using fluorescent tracers, implementing optogenetics in the FIM^{2c} system, imaging *C. elegans* and resolving collisions.

To demonstrate the collision resolution algorithm we extracted posture and motion features for hundreds of collisions. The resultant collision database is currently used to study the behaviour of colliding *Drosophila* larvae [54]. In addition we will utilize the database to implement and test marker-free collision resolution algorithms for future versions of FIMTrack.

APPENDIX

SUPPLEMENTARY MOVIES

To demonstrate the image quality as well as several applications we provide several supplementary movies with this document.

Suppl. Movie 1: General FIM^{2c} Results

FIM^{2c} movie showing 7 wild-type and 7 *daGal4* animals. Note the green fluorescence of the GFP expressing larvae.

Suppl. Movie 2: Exemplary Resolved Collisions

Movie showing several resolved collisions. Note that the outline of the larvae is reduced during animal-animal contacts to highlight the precision.

Suppl. Movie 3: High Resolution Labeled Tissue

nrv2Gal4; UASmGFP third instar larva imaged with UV-light. The movie is taken with 20 frames/s frame rate at a resolution of 380 pixel per larval length. Asterisk denotes segmental abdominal nerves, the arrow highlights an individual *nrv2Gal* positive glial cell. The plus indicates the position of the ventral nerve cord.

Suppl. Movie 4: Optogenetics Using the FIM^{2c} System

nsybGal4; UAS channelrhodopsin expressing animals were raised on all-trans-retinal containing food. A typical seizure behavior is induced upon UV light stimulation. The movie is taken with 20 frames/s frame rate at a resolution of 380 pixel per larval length.

ACKNOWLEDGMENT

The authors are thankful to J. Hermann for help with the construction of the FIM^{2c} setup. We thank J. Krüger and J. Kappel for help with data acquisition. This work was supported by a CIM-IMPRS PhD fellowship to N.O. and through grants of the Deutsche Forschungsgemeinschaft to C.K. (SFB 629 B6, SFB 1009).

REFERENCES

- [1] E. S. Heckscher, S. R. Lockery, and C. Q. Doe, "Characterization of *Drosophila* larval crawling at the level of organism, segment, and somatic body wall musculature." *Journal of Neuroscience*, vol. 32, no. 36, pp. 12460–12471, Sep. 2012.
- [2] I. Schmidt, S. Thomas, P. Kain, B. Risse, E. Naffin, and C. Klämbt, "Kinesin heavy chain function in *Drosophila* glial cells controls neuronal activity." *Journal of Neuroscience*, vol. 32, no. 22, pp. 7466–7476, May 2012.
- [3] A. C. Keene and S. G. Sprecher, "Seeing the light: photobehavior in fruit fly larvae." *Trends in Neurosciences*, vol. 35, no. 2, pp. 104–110, Feb. 2012.
- [4] N. Roussel, C. A. Morton, F. P. Finger, and B. Roysam, "A Computational Model for *C. elegans* Locomotory Behavior: Application to Multiworm Tracking," *IEEE Transactions on Biomedical Engineering*, vol. 54, no. 10, pp. 1786–1797, Oct. 2007.
- [5] K.-m. Huang, P. Cosman, and W. Schafer, "Automated Tracking of Multiple *C. Elegans* with Articulated Models," in *2007 4th IEEE International Symposium on Biomedical Imaging: From Nano to Macro*. IEEE, 2007, pp. 1240–1243.
- [6] Y. Wang and B. Roysam, "Joint tracking and locomotion state recognition of *C. elegans* from time-lapse image sequences," *IEEE International Symposium on Biomedical Imaging: From Nano to Macro*, pp. 540–543, 2010.
- [7] N. A. Swierczek, A. C. Giles, C. H. Rankin, and R. A. Kerr, "High-throughput behavioral analysis in *C. elegans*." *Nature methods*, vol. 8, no. 7, pp. 592–598, Jul. 2011.
- [8] K. Branson, A. A. Robie, J. Bender, P. Perona, and M. H. Dickinson, "High-throughput ethomics in large groups of *Drosophila*." *Nature methods*, vol. 6, no. 6, pp. 451–457, Jun. 2009.
- [9] A. Gomez-Marin, G. J. Stephens, and M. Louis, "Active sampling and decision making in *Drosophila* chemotaxis." *Nature communications*, vol. 2, p. 441, 2011.
- [10] Y. Xiang, Q. Yuan, N. Vogt, L. L. Looger, L. Y. Jan, and Y. N. Jan, "Light-avoidance-mediating photoreceptors tile the *Drosophila* larval body wall." *Nature*, vol. 468, no. 7326, pp. 921–926, Dec. 2010.
- [11] T. A. Ofstad, C. S. Zuker, and M. B. Reiser, "Visual place learning in *Drosophila melanogaster*." *Nature*, vol. 474, no. 7350, pp. 204–207, 2011.
- [12] K. A. Lukyanov, D. M. Chudakov, S. Lukyanov, and V. V. Verkhusha, "Innovation: Photoactivatable fluorescent proteins." *Nature reviews. Molecular cell biology*, vol. 6, no. 11, pp. 885–891, Nov. 2005.
- [13] K. J. T. Venken and H. J. Bellen, "Transgenesis upgrades for *Drosophila melanogaster*." *Development*, vol. 134, no. 20, pp. 3571–3584, Oct. 2007.
- [14] B. Risse, S. Thomas, N. Otto, T. Löpmeier, D. Valkov, X. Jiang, and C. Klämbt, "FIM, a Novel FTIR-Based Imaging Method for High Throughput Locomotion Analysis," *PLoS ONE*, vol. 8, no. 1, p. e53963, Jan. 2013.

- [15] H. Pistori, V. V. Viana Aguiar Odakura, J. B. Oliveira Monteiro, W. N. Gonçalves, A. R. Roel, J. de Andrade Silva, and B. B. Machado, "Mice and larvae tracking using a particle filter with an auto-adjustable observation model," *Pattern Recognition Letters*, vol. 31, no. 4, pp. 337–346, Mar. 2010.
- [16] D. Ramot, B. E. Johnson, T. L. Berry, L. Carnell, and M. B. Goodman, "The Parallel Worm Tracker: a platform for measuring average speed and drug-induced paralysis in nematodes." *PLoS ONE*, vol. 3, no. 5, p. e2208, 2008.
- [17] L. Luo, M. Gershow, M. Rosenzweig, K. Kang, C. Fang-Yen, P. A. Garrity, and A. D. T. Samuel, "Navigational decision making in *Drosophila* thermotaxis." *Journal of Neuroscience*, vol. 30, no. 12, pp. 4261–4272, Mar. 2010.
- [18] S. Khurana, W.-K. Li, and N. S. Atkinson, "Image Enhancement for Tracking the Translucent Larvae of *Drosophila melanogaster*," *PLoS ONE*, vol. 5, no. 12, p. e15259, Dec. 2010.
- [19] C. Sinadinos, C. M. Cowan, A. Wyttenbach, and A. Mudher, "Increased throughput assays of locomotor dysfunction in *Drosophila* larvae," *Journal of Neuroscience methods*, vol. 203, no. 2, pp. 325–334, Jan. 2012.
- [20] E. Yemini, R. A. Kerr, and W. R. Schafer, "Tracking movement behavior of multiple worms on food." *Cold Spring Harbor protocols*, vol. 2011, no. 12, pp. 1483–1487, Dec. 2011.
- [21] M. Gershow, M. Berck, D. Mathew, L. Luo, E. A. Kane, J. R. Carlson, and A. D. T. Samuel, "Controlling airborne cues to study small animal navigation." *Nature methods*, vol. 9, no. 3, pp. 290–296, Mar. 2012.
- [22] X. Cui, L. M. Lee, X. Heng, W. Zhong, P. W. Sternberg, D. Psaltis, and C. Yang, "Lensless high-resolution on-chip optofluidic microscopes for *Caenorhabditis elegans* and cell imaging," *Proceedings of the National Academy of Sciences of the United States of America*, vol. 105, no. 31, pp. 10670–10675, Aug. 2008.
- [23] X. Heng, D. Erickson, L. R. Baugh, Z. Yaqoob, P. W. Sternberg, D. Psaltis, and C. Yang, "Optofluidic Microscopy - a Method for Implementing a High Resolution Optical Microscope on a Chip," *Lab on a chip*, vol. 6, no. 10, pp. 1274–1276, 2006.
- [24] P. Liu, R. J. Martin, and L. Dong, "Micro-electro-fluidic grids for nematodes: a lens-less, image-sensor-less approach for on-chip tracking of nematode locomotion." *Lab on a chip*, vol. 13, no. 4, pp. 650–661, Feb. 2013.
- [25] C. L. Hughes and J. B. Thomas, "A sensory feedback circuit coordinates muscle activity in *Drosophila*." *Molecular and cellular neurosciences*, vol. 35, no. 2, pp. 383–396, Jun. 2007.
- [26] A. Yilmaz, O. Javed, and M. Shah, "Object tracking: A survey," *Acm Computing Surveys (CSUR)*, vol. 38, no. 4, 2006.
- [27] A. J. Spink, R. A. Tegelenbosch, M. O. Buma, and L. P. Noldus, "The EthoVision video tracking system—a tool for behavioral phenotyping of transgenic mice." *Physiology & behavior*, vol. 73, no. 5, pp. 731–744, Aug. 2001.
- [28] A. Gomez-Marin, N. Partoune, G. J. Stephens, and M. Louis, "Automated Tracking of Animal Posture and Movement during Exploration and Sensory Orientation Behaviors." *PLoS ONE*, vol. 7, no. 8, p. e41642, 2012.
- [29] A. P. e. rez Escudero, J. a. n. Vicente-Page, R. C. Hinz, S. Arganda, and G. G. de Polavieja, "idTracker: tracking individuals in a group by automatic identification of unmarked animals," *Nature methods*, pp. 1–9, Jun. 2014.
- [30] L. Fiaschi, F. Diego, K. Gregor, M. Schiegg, U. Koethe, F. Hamprecht, and M. Zlatic, "Tracking indistinguishable translucent objects over time using weakly supervised structured learning," in *IEEE Conference on Computer Vision and Pattern Recognition CVPR, 2014*, 2014.
- [31] J. Ben Arous, Y. Tanizawa, I. Rabinowitch, D. Chatenay, and W. R. Schafer, "Automated imaging of neuronal activity in freely behaving *Caenorhabditis elegans*," *Journal of Neuroscience methods*, vol. 187, no. 2, pp. 229–234, Mar. 2010.
- [32] R. Ardekani, Y. M. Huang, P. Sancheti, R. Stanciuskas, S. Tavaré, and J. Tower, "Using GFP Video to Track 3D Movement and Conditional Gene Expression in Free-Moving Flies." *PLoS ONE*, vol. 7, no. 7, p. e40506, 2012.
- [33] D. Grover, J. Yang, D. Ford, S. Tavaré, and J. Tower, "Simultaneous tracking of movement and gene expression in multiple *Drosophila melanogaster* flies using GFP and DsRED fluorescent reporter transgenes," *BMC Research Notes*, vol. 2, no. 1, p. 58, 2009.
- [34] P. Ramdya, T. Schaffter, D. Floreano, and R. Benton, "Fluorescence Behavioral Imaging (FBI) Tracks Identity in Heterogeneous Groups of *Drosophila*," *PLoS ONE*, vol. 7, no. 11, p. e48381, Nov. 2012.
- [35] N. C. Klapoetke, Y. Murata, S. S. Kim, S. R. Pulver, A. Birdsey-Benson, Y. K. Cho, T. K. Morimoto, A. S. Chuong, E. J. Carpenter, Z. Tian, J. Wang, Y. Xie, Z. Yan, Y. Zhang, B. Y. Chow, B. Surek, M. Melkonian, V. Jayaraman, M. Constantine-Paton, G. K.-S. Wong, and E. S. Boyden, "Independent optical excitation of distinct neural populations," *Nature methods*, vol. 11, no. 3, pp. 338–346, Feb. 2014.
- [36] L. Hernandez-Nunez, J. Belina, M. Klein, G. Si, L. Claus, J. R. Carlson, A. D. T. Samuel, and R. L. Calabrese, "Reverse-correlation analysis of navigation dynamics in *Drosophila* larva using optogenetics," *eLife*, p. e06225, May 2015.
- [37] B. Risse, D. Berh, N. Otto, X. Jiang, and C. Klämbt, "Quantifying subtle locomotion phenotypes of *Drosophila* larvae using internal structures based on FIM images." *Computers in biology and medicine*, vol. 63, pp. 269–276, Aug. 2015.
- [38] B. Risse, N. Otto, D. Berh, X. Jiang, and C. Klämbt, "FIM Imaging and FIMtrack: Two New Tools Allowing High-throughput and Cost Effective Locomotion Analysis," *Journal of Visualized Experiments*, no. 94, pp. e52207–e52207, 2014.
- [39] P. A. Tipler and G. P. Mosca, *Physics for Scientists and Engineers with Modern Physics*, 6th ed. W. H. Freeman, September 2007.
- [40] A. Jain, A. H. J. Yang, and D. Erickson, "Gel-based optical waveguides with live cell encapsulation and integrated microfluidics." *Optics letters*, vol. 37, no. 9, pp. 1472–1474, May 2012.
- [41] H. Bay, A. Ess, T. Tuytelaars, and L. J. V. Gool, "Speeded-up robust features (SURF)," *Computer Vision and Image Understanding*, vol. 110, no. 3, pp. 346–359, 2008.
- [42] M. Muja and D. G. Lowe, "Fast Approximate Nearest Neighbors with Automatic Algorithm Configuration." *VISAPP*, vol. 1, no. 2, pp. 331–340, 2009.
- [43] M. A. Fischler and R. C. Bolles, "Random sample consensus: a paradigm for model fitting with applications to image analysis and automated cartography," *Communications of the ACM*, vol. 24, no. 6, pp. 381–395, June 1981.
- [44] A. H. Brand and N. Perrimon, "Targeted gene expression as a means of altering cell fates and generating dominant phenotypes." *Development*, vol. 118, no. 2, pp. 401–415, Jun. 1993.
- [45] S. Gonzalez-Crespo and M. Levine, "Interactions between dorsal and helix-loop-helix proteins initiate the differentiation of the embryonic mesoderm and neuroectoderm in *Drosophila*." *Genes & development*, vol. 7, no. 9, pp. 1703–1713, Sep. 1993.
- [46] B. Sun, P. Xu, and P. M. Salvaterra, "Dynamic visualization of nervous system in live *Drosophila*." *Proceedings of the National Academy of Sciences of the United States of America*, vol. 96, no. 18, pp. 10438–10443, Aug. 1999.
- [47] P. A. Lawrence, J. Casal, and G. Struhl, "hedgehog and engrailed: pattern formation and polarity in the *Drosophila* abdomen." *Development*, vol. 126, no. 11, pp. 2431–2439, Jun. 1999.
- [48] K. A. Osborne, J. S. de Belle, and M. B. Sokolowski, "Foraging behaviour in *Drosophila* larvae: mushroom body ablation." *Chemical senses*, vol. 26, no. 2, pp. 223–230, Feb. 2001.
- [49] W. W. Ja, G. B. Carvalho, E. M. Mak, N. N. de la Rosa, A. Y. Fang, J. C. Liang, T. Brummel, and S. Benzer, "Prandiology of *Drosophila* and the CAFE assay." *Proceedings of the National Academy of Sciences of the United States of America*, vol. 104, no. 20, pp. 8253–8256, May 2007.
- [50] P. M. Itskov, J. e. M. Moreira, E. Vinnik, G. c. a. Lopes, S. Safarik, M. H. Dickinson, and C. Ribeiro, "Automated monitoring and quantitative analysis of feeding behaviour in *Drosophila*," *Nature communications*, vol. 5, Jul. 2014.
- [51] K. Deisseroth, G. Feng, A. K. Majewska, G. Miesenböck, A. Ting, and M. J. Schnitzer, "Next-generation optical technologies for illuminating genetically targeted brain circuits." *The Journal of Neuroscience*, vol. 26, no. 41, pp. 10380–10386, Oct. 2006.
- [52] C. Schroll, T. Riemensperger, D. Bucher, J. Ehmer, T. Völler, K. Erbguth, B. Gerber, T. Hendel, G. Nagel, E. Buchner, and A. Fiala, "Light-induced activation of distinct modulatory neurons triggers appetitive or aversive learning in *Drosophila* larvae." *Current Biology*, vol. 16, no. 17, pp. 1741–1747, Sep. 2006.
- [53] R. Y. Hwang, L. Zhong, Y. Xu, T. Johnson, F. Zhang, K. Deisseroth, and W. D. Tracey, "Nociceptive neurons protect *Drosophila* larvae from parasitoid wasps." *Current Biology*, vol. 17, no. 24, pp. 2105–2116, Dec. 2007.
- [54] N. Otto, B. Risse, D. Berh, J. Bittern, X. Jiang, and C. Klämbt, "Discrimination of self and non-self in *drosophila* larvae depends on cues before and during collisions," *Journal of Neuroscience*, 2016 under revision.